Journal of The Electrochemical Society, **154** (12) B1227-B1236 (2007)
0013-4651/2007/154(12)/B1227/10/$20.00 © The Electrochemical Society

1D Transient Model for Frost Heave in PEFCs

III. Heat Transfer, Microporous Layer, and Cycling Effects

Suhao He,[a,*] Jong Hyun Lee,[b] and Matthew M. Mench[a,,z]**

[a]*Fuel Cell Dynamics and Diagnostics Laboratory, and Department of Mechanical and Nuclear Engineering, The Pennsylvania State University, University Park, Pennsylvania 16802, USA*
[b]*Hyundai Motor Company, Research and Development Division, Yongin 446-912, Korea*

A computational model based on a frost heave mechanism has been developed to simulate the potential physical damage in polymer electrolyte fuel cells during shutdown to a frozen state. In previous studies by the authors, an analytical model was developed and it was determined that potentially damaging ice lens formation between the catalyst layer and membrane, or between the catalyst layer and the diffusion media under the channel, but not under the landings, can occur under the right conditions. In this study, the role of the microporous layer, multiple cycle accumulated damage, and the direction and rate of heat flux are explored. It was determined that unfrozen water motion occurs toward colder locations during freezing, which can lead to unfavorable ice formation under certain circumstances. The role of the microporous layer on freeze damage mitigation is also important, as it could act to trap liquid water in the catalyst layer. Strategies to mitigate freeze/thaw damage via water removal are proposed, which include controlling the heat transfer direction and rate during shutdown, and the use of engineering materials which facilitate the purging process.
 [DOI: 10.1149/1.2784183]

Manuscript submitted June 3, 2007; revised manuscript received August 8, 2007. Available electronically October 4, 2007.

Recently, the modes of degradation that can occur during freeze/thaw of a polymer electric fuel cell (PEFC) have become a hot topic.[1-16] The freeze/thaw induced damage observed in fuel cell experimental tests has been linked to the residual liquid water by several studies.[1-5,11-16] To determine the root cause of freeze/thaw damage, a frost heave thermal model has been developed by the authors in previous studies,[1-5] and is specifically designed to investigate the potential for ice lens formation resulting from residual water on shut down to a frozen state. The model is based on multiphase porous media flow theories and is a unification and improvement of the rigid ice frost heave model[17-19] and hydraulic frost heave model.[20-23]

In a fuel cell, the frost heave process is a balance between the water drainage and heat dissipation. Specific definitions are discussed here for clarity. We refer to pore ice as ice that accumulates within the pores of the microporous layer (MPL), diffusion media (DM) or catalyst layer (CL), which would typically not cause damage upon shutdown to freezing in an unconstrained situation, since the ice could expand into the structure during the slow freezing process. An ice lens is a sheet-like accumulation of ice commonly observed in soil science, which grows by pulling liquid water into an existing ice formation by capillary forces, and is known to cause delamination or motion between surfaces. In soils, frost heaved surfaces are cracked and elevated. Specifically, an ice lens can continue to thicken when the hydraulic resistance to liquid water flow into the ice location is less than the capillary attractive forces resulting from the freezing process. While pore ice can cause damage in a fully saturated or restrained condition due to expansion, ice lens damage can be formed even with liquids that contract upon freezing,[24] since the underlying physics rely on a balance of capillary forces and heat transfer. The overburden pressure is an important parameter, which is equal to the compressive force on the interface of ice accumulation. Only when the ice phase pressure exceeds the overburden pressure can the ice lens grow, resulting in traditional frost heave. Thus, an ice lens is a unique physical phenomenon that can cause damage independently of the expansion of water on freezing. Low initial liquid saturation, high tortuosity, and mild temperature gradients suppress ice lens formation in porous media. From previous work by the authors, it was predicted that ice lens formation most likely occurs around the catalyst layer, either between catalyst and diffusion media under the channel, or between catalyst layer and Nafion membrane, where the ice phase pressure can overcome the overburden pressure, a contention that is supported by recent experimental studies.[15]

In this study, heat transfer direction, the MPL and cycling effects are investigated. Patterson observed performance loss after freeze-thaw cycles, occurring specifically to the anode end cell of a stack.[25] With the current frost heave model, some of the underlying physics of this phenomenon may now be explained. In addition, the effects of ice lens growth with cycles are detailed, which is similar to what has been observed in soil science, such as the study by Setzer.[26] Finally, ideal materials for avoidance of damage from shutdown to a frozen state can be described with the present model. Cracks common in the catalyst layer, or interfacial gaps between the MPL and catalyst layer, can provide pooling locations with reduced capillary water phase pressure. Water tends to locally accumulate in such locations, and represents a potential source of damage by physical expansion. Although a single cycle would induce too small an ice lens to punch through the DM,[4] repeated cycling of the cell can cause the gap (delamination between DM and CL under channel) to grow. Punch through damage or severe material delamination may occur after many cycles in this way.

Experimental

In the frost heave process, energy and flow equations are strongly coupled with each other, with several strongly nonlinear terms, including a moving freezing front. Problems with moving boundary conditions, such as a melting/freezing front, are usually classified as Stefan problems. Stefan's problem has been studied over several decades, and there are several numerical methods available for solution.[27,28] Besides the moving freezing boundary, frost heave is also a multiphase porous media flow problem. In petroleum engineering, oil-gas-water three-phase flow is commonly modeled using immiscible theory, where it is assumed the multiple phases present do not mix.[29,30] Numerical methods applied include implicit pressure-explicit saturation method, simultaneous solution method, and the sequential method. In civil engineering, immiscible flow theory is commonly used to model the air-water two-phase flow in soil. Since the air phase pressure can be assumed as constant due to low velocity, the flow equations are simplified to Richards equation. There are several numerical methods to solve Richards equation, including Picard iteration, Newton iteration, and some other methods.[31-34]

The frost heave analytical model developed in this work follows individual phase boundaries and is based on immiscible multiphase flow theory. A brief discussion of the most salient aspects of the model is given here, and the reader is referred to previous studies[1-5]

* Electrochemical Society Student Member.
** Electrochemical Society Active Member.
z E-mail: mmm124@psu.edu

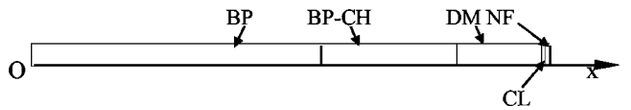

Figure 1. 1D model PEFC geometry.

for more detailed information. By using the finite volume method, the final flow equation derived is like the Richards equation for both saturated and unsaturated domains, and the energy equation in all domains includes a phase-change term, which represents a moving freezing front. The characteristic curves needed for solution, such as the unfrozen water versus water curve and capillary pressure saturation relationship, are taken from available data in literature or thermodynamic relationships, as described in Ref. 1. Some weakly nonlinear but significant terms include liquid advection terms and mixture properties. A Newton solver with global line search ability from Press et al.[35] was used to solve this highly complex nonlinear system of equations. Water phase pressure and temperature of all the nodes, $p_{w,i}$ and T_i, are treated as primary unknowns. They are strongly coupled with the water phase saturation s_w, and ice phase saturation s_i. The energy and flow equations can be written as a set of differential algebraic equations (DAEs).

In the model formulation, the porous material under freezing can transit from liquid to frozen, from saturated to unsaturated, and vice versa. For different states, they have slightly different governing equations, which are updated differently during function evaluation.[1] Appropriate capillary relations are chosen so that all these states form a continuous surface in the capillary pressure-temperature-saturation surface. This also serves as the basis for successful implementation of a Newton solver.[36] With these measures taken, the DAE system can be solved efficiently and accurately.

Figure 1 shows the typical bipolar plate (BP), channel (CH), diffusion media (DM), catalyst layer (CL), and Nafion membrane (NF) one-dimensional (1D) model domain, designated as BP|CH|DM|CL|NF. The model can simulate the bipolar plate interface or channel based on the assigned boundary conditions. In this study, a base line matrix, shown in Tables I and II, was compared to parametric variation of the material properties, geometry, and heat transfer boundary conditions. Some comparative results are shown in Table III.

Results and Discussion

Parametric study: thermal conductivity.— The thermal conductivities of fuel cell components used were taken from manufacturer data or other studies.[37-39] Measured data from Khandelwal and Mench[39] show a significant variance in thermal conductivity with respect to different material types, especially the diffusion media, and is a critical material parameter for water management as well. In this portion of the study, the base case (shown in Table II) is compared with the cases when the conductivity of diffusion media (DM), catalyst layer (CL), or Nafion (NF) has been changed to ten times the base value, respectively, to investigate the potential for altering the freeze behavior with differently engineered materials.

Figure 2 is a schematic of the potential ice lens (IL) locations identified by the analytical model. Note that the model is one dimensional, while Fig. 2 is two dimensional. Simulation of a land and channel condition is accomplished by changing the boundary condition at the interface to either allow or restrict water flux through the boundary. As shown in Fig. 2, IL1 represents a water layer/ice lens at DM|BP or DM|CH interface, IL2 is located at the DM|CL interface, and IL3 is located at the CL|NF interface. IL1 (under the channel) and IL3 (under the land) are positions where ice lens growth is not likely and considered recoverable, since the expansion in the channel is unrestricted and local overburden pressure prevents lens formation and retains materials in position under the land. IL2 (at DM|CL) under the channel is the location where delamination is assumed to be nonrecoverable, where cracks will remain after freeze/thaw cycle due to lower local overburden pressure. Under the channel, the overburden pressure is related to the stiffness of the diffusion media and distributed compression force on the catalyst surface. Pore ice can accumulate from incomplete drainage and re-

Table I. Sensitive input parameters controlling ice lens formation and growth.

Property	Value used for the base case
Water diffusivities of NF[49]	$D_w = \begin{cases} 4 \times 10^{-10}(\lambda/3)^3 & \lambda < 3 \\ 2 \times 10^{-10}(1 + e^{(3-\lambda)/2}) & \lambda \geqslant 3 \end{cases}$
Relative permeability of porous media[48]	$k_{r,w} = s_w^9$
Initial residual water saturation inside porous media at onset of cooldown	0.6 in DM, 0.2 in CL, and $\lambda = 20$ in NF, assumed
Contact angle of fuel cell components	150 for DM, 145 for CL, assumed
Temperature boundary conditions	Natural convection with $h = 0.216$ W/m^2 K, based on a stack thermal parameters
Bipolar plate/open channel boundary conditions	Both
Boundary conditions between CL and NF	$\lambda_{bc} = \begin{cases} 14 + 8s_{w,cl} & \text{nonfrozen CL} \\ \min[14, g(T_{cl})] & \text{frozen CL} \end{cases}$ assumed
Irreducible water content in porous media	0.1 in both DM and CL, assumed

Table II. PEFC component thermal parameters.

	DM[37,39]	CL[39]	NF[39,50,51]
κ, heat conductivity, W/m K	0.14	2.1[a]	0.15
δ, thickness, m	4.0×10^{-4}	1.5×10^{-5}, assumed	5.1×10^{-5}

[a] CL properties are calculated as a mixture of Pt, C, and Nafion with Pt:C:Nafion = 0.32:0.48:0.2 (wt %).

Table III. IL Comparison on IL thickness ratio and pore fill ratio.

		ω		ψ	
		CH, IL2	CH, IL3	BP	CH
Base	Parameter variation	1.00	1.00	0.366	0.366
Thermal conductivity	DM, $\kappa = 10\kappa_0$	1.00	1.00	0.366	0.366
	CL, $\kappa = 10\kappa_0$	1.00	1.00	0.366	0.366
	NF, $\kappa = 10\kappa_0$	1.00	0.30	0.355	0.355
Thickness	DM, $\delta = 2\delta_0$	1.08	1.00	0.368	0.368
	CL, $\delta = 2\delta_0$	0.89	1.00	0.277	0.285
	NF, $\delta = 2\delta_0$	1.49	2.01	0.611	0.612
Thermal boundary condition	$h = 24h_0$	0.52	1.50	0.495	0.496
	Inverted boundary condition	5.10	0.015	0.580	0.617
MPL		0.85	1.00	0.367	0.368

sidual saturation, but should not cause major damage on shutdown due to the long time scale of freeze, unconstrained nature of freeze, and less than fully saturated initial conditions.[c]

The ice lens (IL) thickness ratio and catalyst layer (CL) fill ratios, defined in Ref. 4, are used to evaluate the ice accumulation around the catalyst layer, defined in Eq. 1 and 2.

The ice lens thickness ratio is defined as

$$\omega = \frac{\text{IL thickness for test CH case}}{\text{IL thickness for baseline CH case}} \quad [1]$$

Thus, ω is a measure of the relative thickness of the ice lens found to the base value defined in Table I, and is an indication of ice lens/crack severity.

The CL fill ratio is defined as

$$\psi = 1 - \frac{\text{remaining pore space}}{\text{original pore space}} \quad [2]$$

It is a measure of the total volume available in the CL pores taken by ice. At high ψ, expansion damage is more likely. It is an index of possible ice lens/crack initialization.

Table III shows values of these two parameters for all the simulation tests done for this work. In the base line simulation, the cell at the initial conditions of Table I at a uniform 5°C is subjected to a −5°C left side boundary condition (corresponding to the bipolar plate) at the start time. The mass flux boundary condition at the left side is either simulating the land, in which case mass flux is prohibited, or the channel, in which drainage into low capillary pressure ($P_c = 0$) channel is permitted.

To help understand the results, it is necessary to reiterate the difference between ice lens and pore ice. An ice lens is a result of ice formation and growth resulting from pulling in local water via capillary action. This thin layer of accumulated ice can cause physical damage by displacing materials if the ice phase pressure can overcome the overburden pressure. In soil science, the local overburden pressure is induced by the weight of soil. Here, the overburden pressure is the transmitted pressure and shear restraining capability of the diffusion media. Pore ice is totally different, and is a result of local freezing of water. Pore ice can cause damage via expansion in a confined space.

For damage to occur, there are two possible sources of water: (1) residual DM/CL/MPL water, and (2) electrolyte water. In practice, there can be another key factor, that of commonly observed cracks in the catalyst layer or interfacial sag between the DM and the CL, which can occur with low-stiffness DM structures. Liquid water in such cracks is especially difficult to efficiently purge, and can remain as a source of liquid in contact with the electrolyte and pore expansion damage during shutdown until the freezing point is reached, unless removed by purge or evaporation. This situation is especially difficult with MPLs, since the catalyst layer water can be trapped between this highly hydrophobic layer until high saturation occurs. Catalyst layer cracks have been observed to exacerbate physical damage in ex situ freeze/thaw testing.[15] In this work, Kim and Mench subjected membrane electrode assembly (MEA) materials with diffusion media and microporous layers to repeated freeze/thaw cycling from −40°C to 70°C in an ex situ submerged liquid environment. After 30 cycles, damage to the MEAs with cracks in the virgin catalyst layer was significantly more severe than those of MEAs without cracking in the virgin catalyst layer. Figure 3 shows the comparison results for the final pore ice saturation in the DM and electrolyte for different thermal conductivity values. Figure 3a is for a location under the land, while 3b is for a location under the channel, where liquid is allowed to drain. Since this model is 1D, the high capillary pressure in Fig. 3a will not force lateral transport under the land into the channel DM, and thus the final pore ice saturation is overestimated, but still not high enough to cause expected damage.

From the generalized Clapeyron equation,[40] when unfrozen water is equilibrated with ice, one has

$$\frac{p_i}{\rho_i} - \frac{p_w}{\rho_w} = -h_{sf}\left(\frac{T - T_f}{T_f}\right) = -h_{sf}\left(\frac{\Delta T}{T_f}\right) \quad [3]$$

If ice phase pressure is assumed constant at the overburden value when frost heave occurs (e.g., $p_i = p_{ovbd}$), one can derive

$$\nabla p_w = \frac{h_{sf}\rho_w}{T_f} \nabla T \quad [4]$$

From this, the gradient of water phase pressure is proportional to the gradient of temperature. Thus, with higher temperature gradient between the liquid water source and the ice location, one can expect more water flux into the ice lens driven by the water phase pressure.

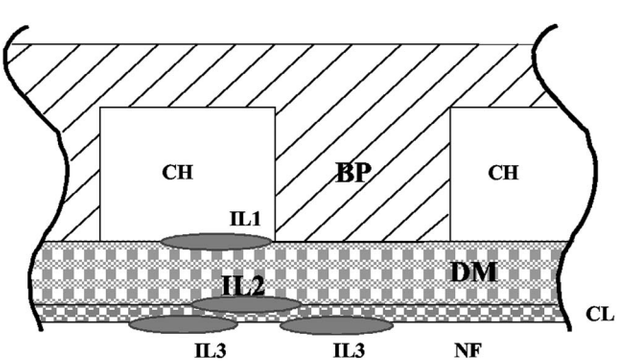

Figure 2. Illustration showing locations of IL1, IL2, and IL3.

[c] This model does not consider damage relating to start-up, where super cooled water may exist, and extremely rapid freezing can occur.

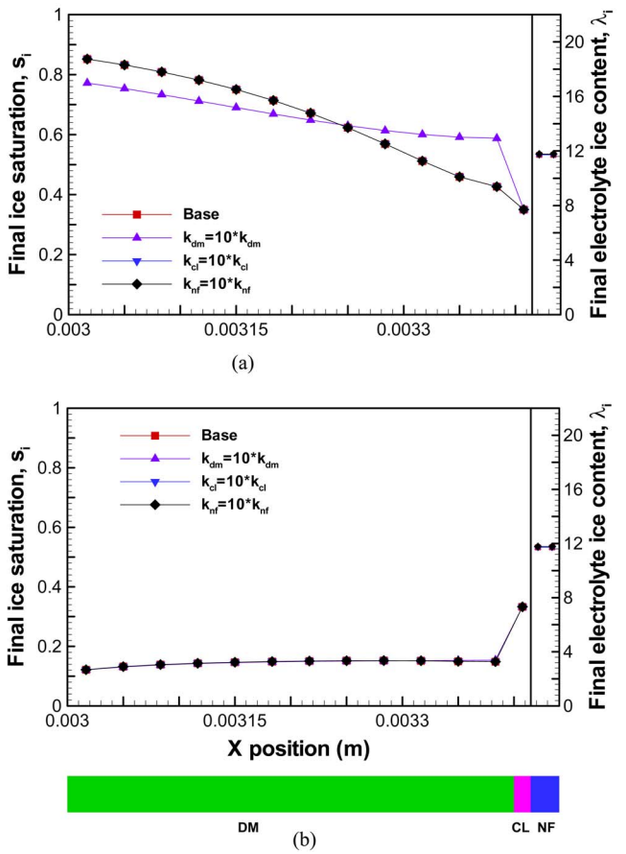

Figure 3. (Color online) Comparison on final pore ice saturation for cases with different material thermal conductivity, when the membrane electrolyte assembly is (a) under the BP and (b) under the CH.

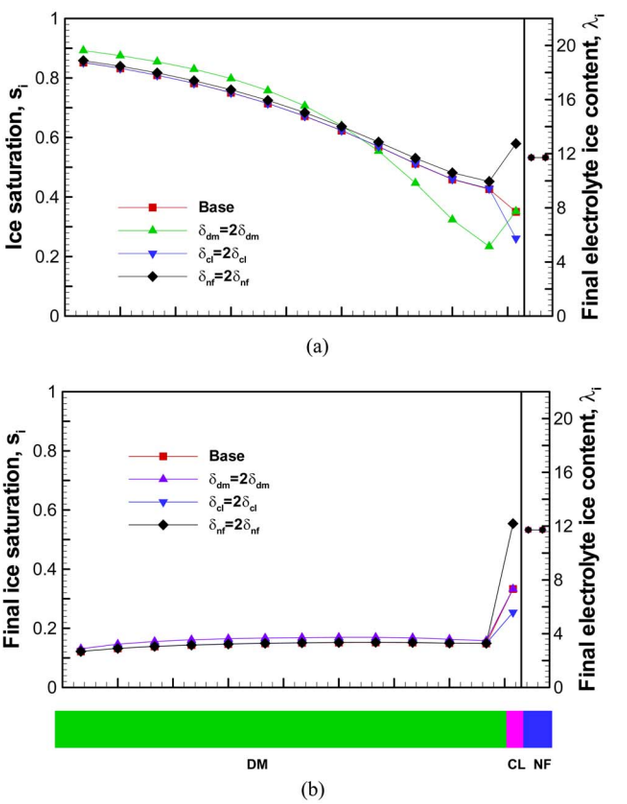

Figure 4. (Color online) Comparison on final pore ice saturation for cases with different material layer thickness when the membrane electrolyte assembly is (a) under the BP and (b) under the CH. (The three cases are with different layer thickness, so the saturation distribution has been stretched to fit the geometry shown in the bar so that they are comparable.)

The total unfrozen water migration into the ice lens, or ice lens growth, depends on this pressure gradient, the relative permeability of the unfrozen water, and the total freezing time.

The overall heat dissipation rate at the left DM boundary is comparable for all three cases in Fig. 3, so that a higher material conductivity results in a reduced temperature gradient within the material. As shown in Fig. 3a, as a result the case with higher DM conductivity shows less unfrozen water transport to the left before freezing under the land, but not much difference under the channel, since porous media drainage to nearly the irreducible saturation values is much faster than the freezing process in this situation. This also indicates the importance of the irreducible saturation value to control residual ice content, reduce purge requirements, and accelerate start-up from frozen conditions. Similarly, one would expect an increase in CL conductivity will result in less unfrozen water from CL to DM or IL2. But this effect is not noticeable from Table III, because the quantity of unfrozen water flow from CL is very small. However, an increase in NF thermal conductivity induces a decrease of IL3 under the land, a location unlikely to suffer any permanent damage due to the high overburden pressure. The lack of damage under the land location has recently been validated by ex situ material studies.[15]

Parametric study: diffusion media, catalyst layer, and electrolyte thickness.— Figure 4 shows the comparison of the final pore ice between the base case and the cases with doubled material layer thickness, for DM, CL, and NF layer, respectively. Table III shows the final results for the CL filling and ice lens thickness. Results show that the ice saturation in the CL decreases with doubled CL thickness and increases with doubled NF thickness, which is also shown in Table III. This indicates that ice accumulation in CL is mainly from the electrolyte as a source. Doubled NF thickness means a greater water source and doubled CL thickness means more storage room for pore ice accumulation, and also a reduced temperature gradient, similar to an increased thermal conductivity effect. The present 1D model assumes a homogeneous initial water distribution inside the porous materials. Also assumed is a pseudo-thermodynamic equilibrium at each time step. Before freezing, water under the channel will drain to almost irreducible water content since the time scale of drainage is much smaller than that of heat transfer.[d] Upon freezing, water inside the DM and CL will all freeze within their freezing temperature depression. The formed pore ice usually will not saturate the pores in DM and CL at that point. However, some of the water in Nafion has a broad freezing temperature depression.[41] The present model allows the unfrozen water inside Nafion to flow out, driven by a water concentration gradient from a diffusion model. This results from Schroeder's Paradox, when some portion of the electrolyte is in contact with liquid water, and a discontinuity of water uptake is observed.[42] From this approach, one would expect the unfrozen water below 0°C to flow out of Nafion and then freeze instantly at the CL|NF boundary, potentially causing interfacial damage. Another possible explanation for this delamination is ice formation and volume change of the Nafion itself. Our group has recently shown that delamination at the CL|NF

[d] Note that the model allows complete drainage of the DM under the channel into the channel. In practice, the presence of a droplet or film on the channel can prohibit the further drainage of the DM water by increased capillary pressure in the covering liquid mass. Thus, complete drainage of the DM under the channel may be accomplished as long as there is no blocking effect by channel water.

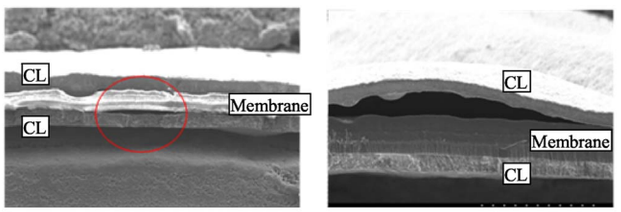

Figure 5. (Color online) Comparison of freeze thaw damage from thermal cycling from −40 to 70°C with (a) an 18 μm reinforced membrane electrode assembly with no initial cracks in the virgin catalyst layer, and SGL 10BB diffusion media with MPL and (b) a 35 μm reinforced membrane electrode assembly with no initial cracks in the virgin catalyst layer, and SGL 10BB diffusion media with MPL, taken from Ref. 15.

interface indeed can occur as a result of a membrane water source, independent of the diffusion media water. It has been confirmed that a thicker membrane results in greater delamination,[15] as predicted here and shown experimentally in Fig. 5. A recent paper by Pineri et al.[43] showed some X-ray diffraction results, which indicate that part of water desorbs out of the membrane below 0°C and water never crystallizes inside. This suggests that the damage is more likely a result of water outflow than NF expansion. But the end result for both cases is the same, that a source of potential damage is excess membrane water resulting from liquid water in contact with the electrolyte at shutdown to a frozen state.

Parametric study: thermal boundary conditions/end cell effects.— The base line thermal boundary condition for the 1D model is convective heat transfer at the BP (left) side and zero heat flux at the NF (right) side of Fig. 1. In a practical stack application, the heat transfer direction can be reversed from this, depending on the plate location in the stack, as illustrated in Fig. 6. To study the end cell effects in stacks, additional simulations with zero heat flux at the bipolar plate (left) side were conducted with the heat flux out of the electrolyte (right) boundary. To study the influence of geometry, heat flux direction and rate, and the microporous layer (MPL), the relevant parameters in the numerical model were changed.

The boundary conditions for the base line case are convective heat transfer with a heat transfer coefficient chosen so that the cell has a characteristic freeze time of 24 h, to simulate a real stack cooling-down process. Simulations were also conducted with a convective heat transfer coefficient 24 times the original value, so the cell has a characteristic freeze time of 1 h, similar to a laboratory-based single cell test condition.

Figure 7 shows the final pore ice resulting from a parametric study with these combinations of thermal boundary conditions (laboratory vs automotive time scale and toward or away from the bipolar plate). For faster laboratory-based cooling, one can observe more water flux toward the cold side, induced by the higher temperature gradient. This effect may be important to interpret lab results from rapid freeze/thaw cycling. The use of rapid thermal cycling may overestimate the damage caused in the real stack, when additional drainage before freezing will reduce water sources for ice

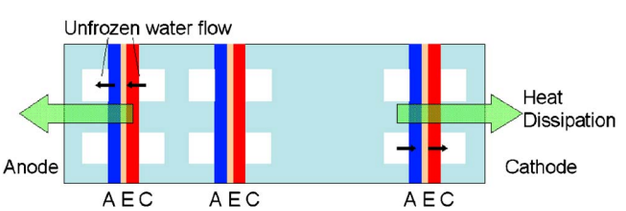

Figure 6. (Color online) Illustration showing stack structure and unfrozen water flow in a fuel cell stack.

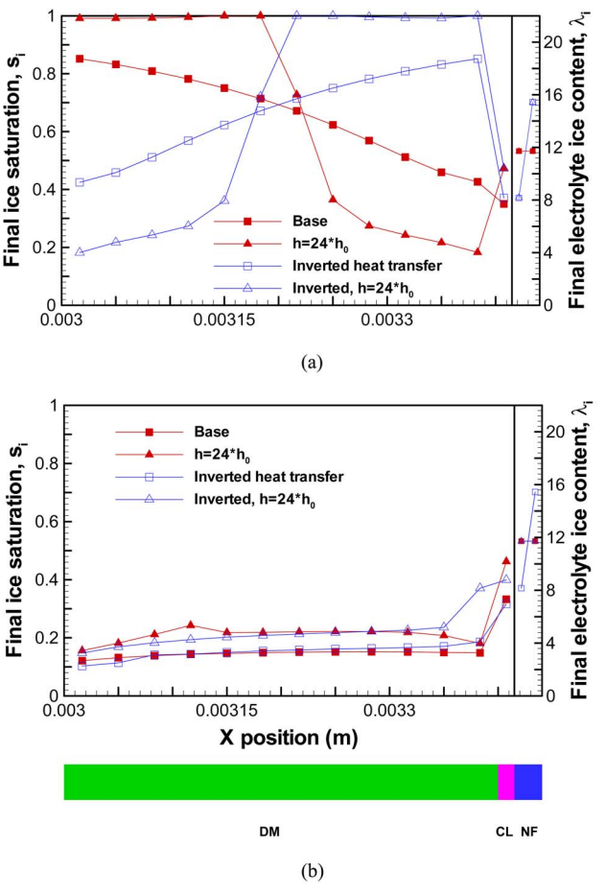

Figure 7. (Color online) Comparison on final pore ice saturation for cases with different thermal boundary conditions when the membrane electrolyte assembly is (a) under the BP and (b) under the CH.

damage. As a result of the temperature gradient dependency, one would generally expect more unfrozen water migration toward the cold end (anode end) of the stack. At this location, residual water in the cathode side of these cells would tend to migrate toward the catalyst layer during freezing. Provided there is typically more residual water at the cathode side, this situation may be linked to the end cell effects observed in Patterson's study.[25] As addressed by Patterson, the anode end cell suffered more performance loss than the cathode end cell during freeze/thaw cycling. This is strong evidence that residual water and temperature gradient have direct impacts on the freeze/thaw-induced damage.

For the inverted heat transfer case, unfrozen water flow is now toward the CL, which gives a higher final ice accumulation in the CL. Note that (a) the unfrozen flow is a result of capillary forces generated by phase change, different than the temperature gradient (without phase change) induced motion observed by Bradean and co-workers[44] and Zaffou and co-workers,[45] and (b) the model does not consider mass transfer out of the membrane (right) side of the domain, although water could be driven across the boundary in practice. This important consideration is part of continuing study, since the water buildup at the catalyst layer could be drained and flow toward the other side if mass transfer across the membrane is allowed. It should be noted that thermo-osmosis is different from the phase-change induced migration modeled in this work. The thermo-osmosis effect occurs without phase change under a temperature gradient. There is still some discrepancy in the literature about the thermo-osmosis effect in the membrane, however. Typically, water in hydrophilic media flows under a temperature gradient toward the

Table IV. MPL physical properties.[52,53]

Property	Value
Thickness, m	30
Porosity	0.4 or 0.5
Pore size, nm	250
Permeability, m^2	2.5×10^{-14}
Contact angle, degree	150
Thermal conductivity, W/m K	0.4
Specific heat, J/kg K	710
Freezing temperature depression, °C	0.96

warmer location, which has been observed for some membranes[45] but for a fuel cell MEA with diffusion media, the opposite has been observed.[44] More fundamental study of this interesting phenomenon is needed to fully explain this discrepancy. Interestingly, the approach to mitigate damage from the residual liquid using a temperature gradient can either be to restrict access to the catalyst layer by incorporating a more tortuous DM at the end cells as Patterson and others at UTC have discussed,[25] or intentionally increasing the temperature gradient near the cold anode end cells to drain the residual water through the MEA into the anode channel as discussed by Bradean.[44]

For natural heat transfer cooling from a fuel cell stack, the end cells have the highest temperature gradient during cooling, which means the highest unfrozen water flux before and during freezing. Focusing on the anode and cathode end cell, water is generated at the cathode catalyst layer and condensed to liquid form if the conditions become supersaturated. One of the major roles of the diffusion media is to remove this product water to the channel and prevent blocking of the reactant to the catalyst layer. When liquid water accumulation reaches a certain level, reactant gas is blocked from penetrating to the catalyst surface. Although channel level flooding is commonly observed, especially in the anode at low current density, the DM/CL water generally increases as the current density increases and is more predominant under the lands.[46,47] Upon shutdown from a moderate or high current condition, the cathode will then typically have more residual water than the anode, especially in the diffusion media.

Due to the unfrozen water flow driven by the temperature field, this could make a significant difference between the anode end cell and cathode end cell situation. In the anode end cell, the residual water in the cathode will flow toward the cathode catalyst layer. In the cathode end cell, the residual water in the anode will flow toward the catalyst layer. However, one can expect more residual water for the first case. Thus, more unfrozen water flows from the cathode toward the cathode catalyst layer for the anode end cell, which means a greater potential damage in the cathode catalyst layer, since water accumulation in catalyst layer directly relates to potential damage. Thus, restriction of liquid entry to the catalyst layer on the anode side with material modifications or removal of the residual water on shutdown can be used to mitigate this damage mode.

With respect to fuel cell performance on start-up, with more ice accumulation in catalyst layer, there is more ice to melt during cold start. Together with newly generated water, flooding would more easily occur on start-up at these locations of heat flux driven flow into the catalyst layer.

MPL study.— A highly hydrophobic, thin microporous layer (MPL) between the catalyst layer and the diffusion media is often used for water management, enhanced electrical conductivity, and protection of the catalyst layer from stiff fiber intrusion, but has not been included in the simulations discussed so far. Since the MPL has much smaller pores than the DM and is nearly completely hydrophobic, it has an elevated liquid-phase pressure for the same saturation level as the surrounding porous media and catalyst layers. Table IV shows some typical parameter values for the MPL used in the present study.

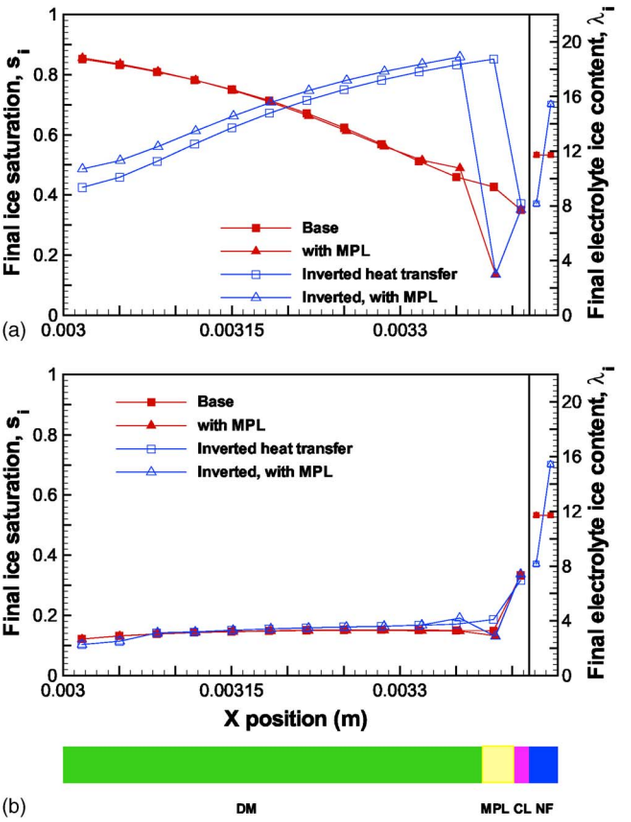

Figure 8. (Color online) Comparison on final pore ice saturation for the base case and the cases with MPL, when the membrane electrolyte assembly is (a) under the BP and (b) under the CH.

To examine the effects of the MPL layer on the final ice distribution and pore ice content, the original 400 μm DM was changed into a 370 μm DM combined with a 30 μm MPL in the simulations. Figure 8 shows final residual pore ice with and without MPL, and Table III shows the ice lens and CL pore filling data comparison data. With an inverted thermal boundary condition, the unfrozen water flows into the catalyst layer, but note that the overall effect of the MPL is a low saturation region in front of the catalyst layer.

Cycling effects.— When the fuel cell is cycled, a small delamination between the layers under the channel could be nonrecoverable if the DM material plastic deformation limits are reached. In each cycle, residual water will tend to accumulate at these gap locations due to locally lower water phase pressure, and will only be removed by evaporative or forced convective forces and not capillary forces. As previously discussed, unless there is a defect, the interfacial gap between the CL and DM is small for a single cycle but can grow over many cycles, leading to gap expansion. A stiff DM can also provide a distributed overburden pressure, restricting the initial ice growth. Another possibility is similar to lateral crack expansion that occurs in roads and other structures under repeated freezing conditions. Cracks in the virgin catalyst layer can be expanded by pooled water freezing, and cause local damage during freeze cycling.

For the cycling study here, delamination at the CL|DM interface under the channel is considered as unrecoverable. For simulation of multiple cycles, an initial gap at the onset of each cycle is set at CL|DM interface with its thickness equal to the final ice lens thickness from the last cycle. It is assumed that the gap is initially filled with water, due to low local water phase pressure. In practice, the

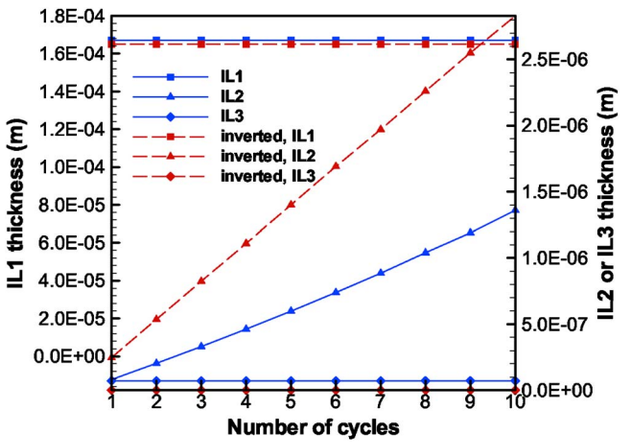

Figure 9. (Color online) Illustration showing ice lens growth during cycling.

small initial ice lens formed per cycle may not cause permanent deformation, so this simulation is a worst-case scenario.

Figure 9 shows the simulation results on cycling effects for the base case and inverted boundary condition. The ice lens 2 (IL2) location between the CL and DM under the channel delamination grows with cycles almost linearly, and much more rapidly in the inverted thermal boundary condition (cold toward the membrane). The channel ice (IL1) and under the land ice lens (IL3) are constant since the drainage into the channel does not change and land compression prevents expansion, respectively. The more ice lens growth for a single cycle (i.e., the greater water source), the faster the total delamination grows. However, it should be pointed that since most of the DM|CL drainage occurs before freezing, the total IL thickness is very small, so that significant damage would occur over tens or hundreds of cycles in this mode. This also highlights the importance of prevention of DM sag into channels over time, and the need for some purge on shutdown to remove residual pooled water in cracks or gaps.

From the parametric study results, for a single cycle, CL hydrophobicity, porous material drainage speed, CL irreducible water content, NF thickness, cooling rate and direction, and the MPL addition are the most important factors determining the final ice accumulation around the catalyst layer. Figures 10a and b show the change of IL2 thickness ratio (ratio of IL2 to base line IL2 case) with cycles for (a) base line and (b) inverted thermal boundary conditions with variations in irreducible saturation, heat transfer rate and direction, drainage rate, hydrophobicity, and membrane thickness. The IL2 thickness ratio is an index showing the proclivity for damage at DM|CL interface under the channel. The growth of this index directly relates to the growth of delamination or expansion cracks. It is found that, among the parameters chosen for study, the most important parameter in the base line case is the drainage rate of the medium, which is really an unknown relationship between the relative permeability of the porous medium and saturation. It is not appropriate to use the $k_{r,w} = s_w^3$ relationship commonly employed in fuel cell literature, because the ice phase represents an additional resistance to liquid flow. A ninth order relationship applied in the simulation has been suggested by some[48] e.g., $k_{r,w} = s_w^9$, as well as inclusion of the ice phase saturation in some form, which is more appropriate physically, but much more cumbersome computationally. For the inverted heat transfer boundary condition cases, the drainage rate is also important, but the heat transfer rate is even more critical in IL2 growth. In this case, the laboratory scale freezing time has a greater impact, trapping more liquid water in the porous media.

Typically, the drainage speed is much faster than heat transfer so that before the DM freezes, the water has drained to nearly a residual level (unless the channel is blocked with slugs), regardless of

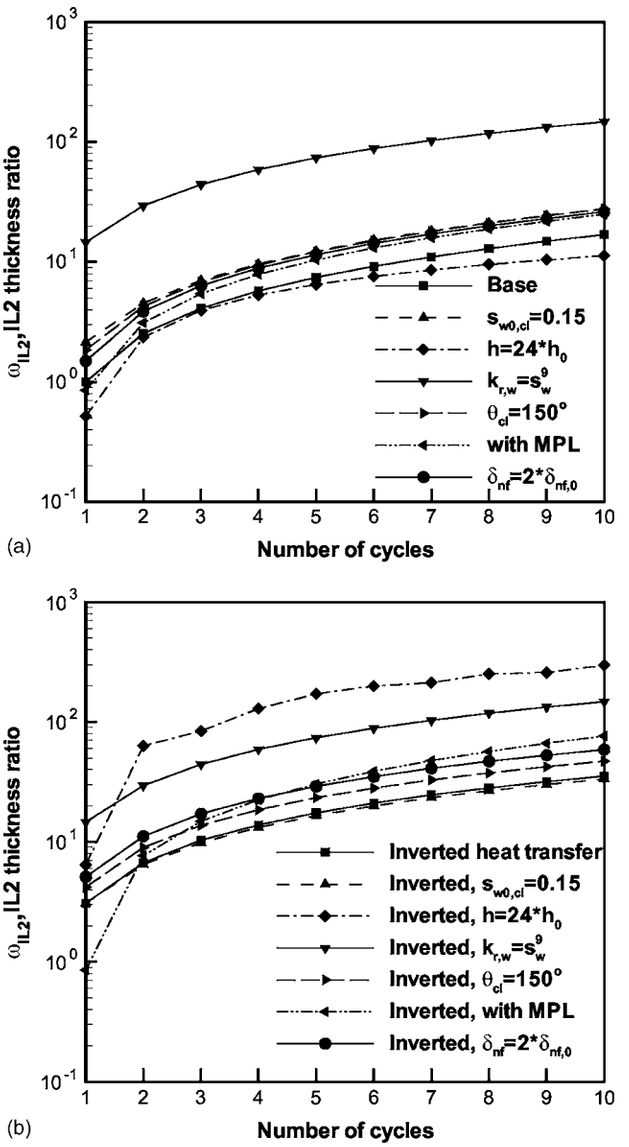

Figure 10. IL2 thickness ratio change with cycles with (a) base and (b) inverted thermal boundary conditions.

whether the heat transfer has been inverted. In Fig. 8, it can be seen that the heat transfer direction makes some difference on the final ice saturation in CL, but not much due to the high water phase pressure for a given saturation level in the small-pore size catalyst layer. When there is an ice lens between the DM and IL, however, the IL growth rate can be very different, as we can observe in Fig. 10.

Figure 11 shows the change of catalyst pore ice fill ratio with cycles. The pore ice fill ratio (ψ) actually considers not only the pore ice, but also the ice lens at DM|CL and CL|NF interfaces, so that it can exceed 1.0. It is an index addressing the total amount of ice around the catalyst layer

$$\psi = s_{i,\mathrm{cl}} + \frac{\delta_{il2} + \delta_{il3}}{\varepsilon_{cl}\delta_{cl}} \qquad [5]$$

Here, $s_{i,\mathrm{cl}}$ is final ice saturation in catalyst layer; δ_{il3} is the calculated ice lens thickness at the NF|CL interface, which can also possibly contribute through expansion; δ_{il2} is the ice lens thickness at DM|CL, included here since the interface at DM|CL is not distinct;

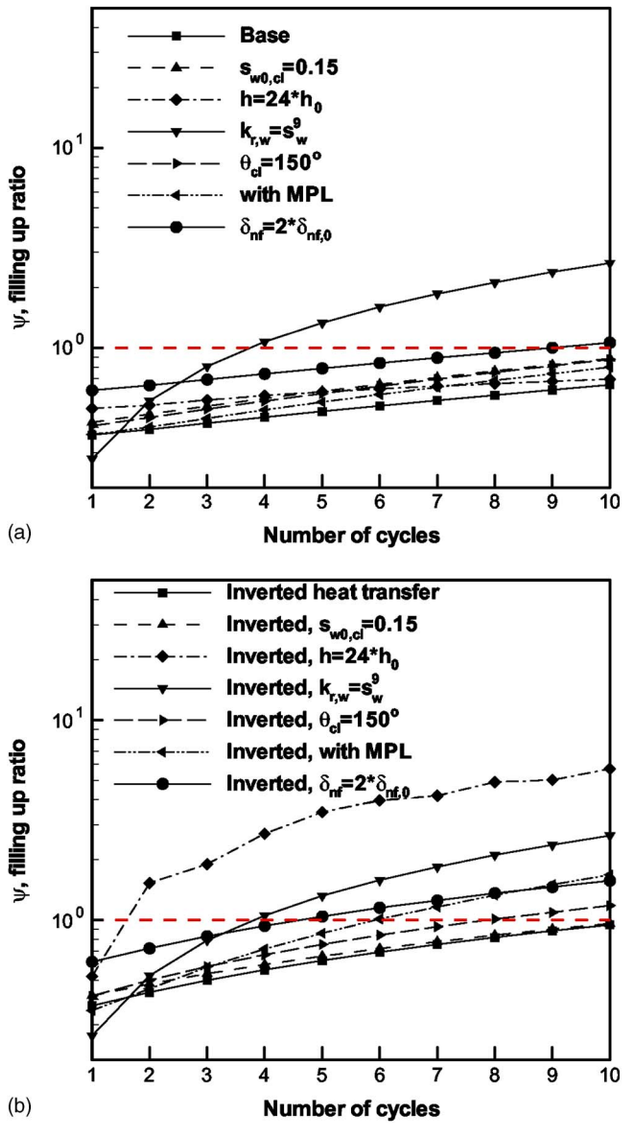

Figure 11. (Color online) Catalyst pore ice fill ratio change with cycles with (a) base and (b) inverted thermal boundary conditions.

ε_{cl} is the porosity of catalyst layer and δ_{cl} is thickness of catalyst layer. The second part of Eq. 5 is usually a very small value, ~0.01, but can be larger, if catalyst layer cracking effects are included. The higher the index, the higher proclivity for damage to occur. Also note that an index bigger than unity does not necessarily guarantee damage, since it includes water from the ice lenses as well as CL pore ice.

From Fig. 11, the worst cases are for slow drainage rates and inverted, rapid cooling conditions, similar to Fig. 10. The case with MPL and inverted heat transfer also has a relatively high fill ratio after cycles. The reason is that for the same amount of water, the MPL tends to have higher water phase pressure than DM. So there will be more unfrozen water flow into the IL at MPL|CL interface than the DM|CL interface when heat transfer conditions are inverted.

Controlling strategies.— From previous discussions, ice damage can be caused by a high pore ice saturation, and ice lens formation under the channels. The major sources of water causing this damage are electrolyte water[1,15] and residual water in the catalyst layer cracks or interfacial gaps. The ultimate solution to avoid any freeze/thaw damage would be elimination of all liquid water contact with the electrolyte, preventing the excess water uptake via Schroeder's Paradox, while maintaining a fully or at least partially hydrated electrolyte, since severe dehydration of the electrolyte would reduce electrolyte conductivity at start-up, can cause degradation itself, and is usually parasitic to achieve.

Strategies to control these damages can be designed based on the general idea to reduce or eliminate the two sources of damaging water: (1) excess liquid water in the electrolyte and (2) residual liquid in the CL and DM.

Heat transfer.— As explained in previous discussion, the temperature gradient directly relates to the unfrozen water flow. To control the temperature gradient and direction becomes important, especially around the places where the ice lens is likely to form. In general, a higher temperature gradient during freezing will induce more unfrozen water flux toward the cold location, in the time scales typical of fuel cell stack cooling. If the cell were instantaneously frozen, there would not be enough time for this phase change based water flux to form ice lenses, and only pore-level expansion damage would result.

Purge.— Drainage into the channel locations is critical to reduce the diffusion media and electrolyte water sources, and a perfect purge based on a flow of dry gases would eliminate issues with shutdown to a frozen state, but is highly parasitic, slow, and can also cause damage from relative humidity cycling. After shutdown of a fuel cell, there is residual liquid water in the flow channel, within porous materials, and potentially inside the electrolyte. Any reduction in the liquid contact with the electrolyte will reduce frozen damage from this source. To dry out the cell components, especially the electrolyte, would help prevent freeze/thaw damage, but even some removal of the channel-level water is critical at shutdown (as per a brief blast of channel flow after cooldown but above freeze). Removal of the first layer of channel water that drains from the DM allows additional diffusion media water to fully drain from both the channel and land. Since the DM liquid water will self-drain to residual saturation levels (related to hydrophilic pore volume) into an unflooded channel given enough time, it is critical to purge liquid water removal from the catalyst later, which can be hindered by the presence of a highly hydrophobic microporous layer. This can be accomplished via evaporation, and other parasitic and nonparasitic methods beyond the scope of this paper.

Materials.— To control freeze/thaw damage, virgin catalyst layer cracks should be eliminated. Porous material with less irreducible water saturation (e.g., higher hydrophobicity) are favored. Similarly, a thinner electrolyte material with less expansion is also favored to reduce initial water content and potential expansion damage. A stiff diffusion media structure can also reduce interfacial gaps and apply some overburden pressure on the catalyst layer, restricting ice lens formation.

Drainage speed can be tailored by tortuosity, pore size and polytetrafluoroethylene content. A fast drainage rate means less time is required to drain residual water. If purging is not very successful, and liquid water remains trapped in the DM by channel level slugs, fast drainage will be detrimental, since it facilitates unfrozen water flow toward the ice lens. The MPL shows some varied effects. On one hand, the low water saturation in the MPL and high hydrophobicity helps to prevent unfrozen water flow from the DM through the MPL into a freezing CL. On the other hand, liquid water trapped in the CL after shutdown will not easily pass through the MPL on purge and can be trapped in the CL, exacerbating damage potential.

Design.— The fuel cell design itself plays an important role in the water retention in the porous media. The geometry, surface properties, heat transfer characteristics can be engineered to reduce steady state water content and enhance natural drainage. Since the diffusion media area under the land tends to retain a higher saturation than under the channel,[46] a high channel to land ratio can be used to reduce water content carried in the cell under normal oper-

ating conditions. Additionally, the landing/diffusion media interface plays an important role in facilitating water removal from under the land, and geometric techniques or surface coatings can be applied to enhance this function and also reduce water content. Finally, the heat transfer rate and direction of the cells in the stack can be adjusted to better remove product water storage.

Conclusion

This study discussed the effects of thermal parameters, geometry, a microporous layer (MPL), and cycling on freeze/thaw damage. Two main sources of ice lens water were found (1) residual water in the catalyst layer and diffusion media and (2) excess water in the electrolyte. During freezing, the driving force of unfrozen water flow is proportional to the temperature gradient between the ice and the liquid water, with unfrozen flow toward the cold location. Several factors were found to exacerbate ice lens initialization and growth under the channel location including a rapid heat transfer process, slower liquid drainage into the channel, cooling toward the catalyst layer, and a high irreducible liquid saturation. Also, increasing material thermal conductivity reduces the temperature gradients, decreasing ice lens growth. It was also determined that increasing the electrolyte thickness would cause a greater source for ice growth and potential delamination, which has been confirmed by experimental study. In terms of pore ice, there is generally enough space for unrestrained expansion without reaching saturation levels where damage would be likely from simple expansion, unless a high initial saturation remains trapped between the MPLs.

The role of the MPL is mixed. While the MPL can block unfrozen water flow from the DM toward CL, it also restricts drainage of liquid water from the catalyst layer without evaporation. The effects of multiple freeze thaw cycles can be cumulative if the gap space between the catalyst layer and diffusion media plastically deforms and grows. This interfacial gap can act as a pooling location for future cycles, accumulating further damage. Various general control approaches were proposed based on the simulation results. In general, methods should be aimed to decrease residual liquid water contact with the electrolyte and use of robust materials. Damage mitigation can be accomplished by various modes of purging, control of the heat transfer rate and direction during shutdown, and use of engineering materials such as a crack-free catalyst layer and stiff diffusion media without interfacial gaps or sag under the channels.

Acknowledgments

This research was supported by the Advanced Technology Center, R&D Division for Hyundai Motor Company & Kia Motors Corporation (HMC&KMC). The help of Professor Patrick Reed of Penn State Department of Civil and Environmental Engineering in suggesting methods to computationally solve the formulated model is also gratefully acknowledged.

The Pennsylvania State University assisted in meeting the publication costs of this article.

List of Symbols

D	diffusivity, m/s^2
$g(T)$	unfrozen water vs temperature curve for NF
h	convective heat transfer coefficient, W/m^2 K
h_{sf}	heat of fusion, J/Kg
k	permeability, m^2
k_r	relative permeability
p	phase pressure, Pa
p_{ovbd}	overburden pressure, Pa
s	saturation
s_{w0}	irreducible water saturation
T	temperature, K
T_f	reference freezing temperature, 273.15 K
ΔT	freezing temperature depression, K

Greek

δ	thickness, m
ε	porosity
κ	thermal conductivity, W/m K
λ	water content in Nafion, mol H_2O/mol SO_3^-
θ	contact angle, degree
ρ	density, kg/m^3
ω	IL thickness ratio
ψ	fill ratio

Subscripts

0	reference point
bc	boundary condition
cl	catalyst layer
dm	diffusion media
i	ice phase
il	ice lens
nf	Nafion
w	water phase

References

1. S. He and M. M. Mench, *J. Electrochem. Soc.*, **153**, A1724 (2006).
2. M. M. Mench and S. He, *ECS Trans.*, **1**(8), 415 (2006).
3. M. M. Mench and S. He, *ECS Trans.*, **3**(1), 897 (2006).
4. S. He, S. H. Kim, and M. M. Mench, *J. Electrochem. Soc.*, **154**, B1024 (2007).
5. S. He, Ph.D. Thesis, The Pennsylvania State University, University Park, PA (2007).
6. M. S. Wilson, J. A. Valerio, and S. Gottesfeld, *Electrochim. Acta*, **40**, 355 (1995).
7. R. C. McDonald, C. K. Mittelsteadt, and E. L. Thompson, *Fuel Cells*, **4**, 208 (2004).
8. L. Blair, in *Proceedings of Fuel Cell Operations at Sub-Freezing Temperatures Workshop*, http://www.eere.energy.gov/hydrogenandfuelcells/fc_freeze_workshop.html (2005).
9. E. Cho, J.-J. Ko, H. Y. Ha, S.-A. Hong, K.-Y. Lee, T.-W. Lim, and I.-H. Oh, *J. Electrochem. Soc.*, **150**, A1667 (2003).
10. E. Cho, J.-J. Ko, H. Y. Ha, S.-A. Hong, K.-Y. Lee, T.-W. Lim, and I.-H. Oh, *J. Electrochem. Soc.*, **151**, A661 (2004).
11. B. Pivovar, in *Proceedings of Fuel Cell Operations at Sub-Freezing Temperatures Workshop*, http://www.eere.energy.gov/hydrogenandfuelcells/fc_freeze_workshop.html (2005).
12. Q. Guo and Z. Qi, *J. Power Sources*, **160**, 1269 (2006).
13. J. P. Meyers, in *Proceedings of Fuel Cell Operations at Sub-Freezing Temperatures Workshop*, http://www.eere.energy.gov/hydrogenandfuelcells/fc_freeze_workshop.html (2005).
14. S. He, S. H. Kim, and M. M. Mench, *J. Electrochem. Soc.*, Submitted.
15. S. Kim and M. M. Mench, *J. Power Sources*, In press.
16. J. Hou, H. Yu, S. Zhang, S. Sun, H. Wang, B. Yi, and P. Ming, *J. Power Sources*, **162**, 513 (2006).
17. R. D. Miller, in *Proceedings of the Third International Conference on Permafrost*, p. 708, National Research Council of Canada, Ottawa, Ont., Canada (1978).
18. K. O'Neill and R. D. Miller, *Water Resour. Res.*, **21**, 281 (1985).
19. P. B. Black, CRREL Report 95-12, p. 1, U.S. Army Cold Region Research and Engineering Laboratory, Hanover, NH (1995).
20. R. L. Harlan, *Water Resour. Res.*, **9**, 1314 (1973).
21. Y. W. Jame and D. I. Norum, *Water Resour. Res.*, **16**, 811 (1980).
22. G. P. Newman and G. W. Wilson, *Can. Geotech. J.*, **34**, 63 (1997).
23. L. Zhao and D. M. Gray, *ASME, Heat Trans. Div.*, **331**, 53 (1996).
24. T. Mizusaki and M. Hiroi, *Physica B*, **210**, 403 (1995).
25. T. Patterson, in *2006 U. S. DOE Annual Program Review Proceedings*, http://www.eere.energy.gov/hydrogenandfuelcells (2006).
26. M. J. Setzer, *J. Colloid Interface Sci.*, **243**, 193 (2001).
27. C. R. Swaminathan and V. R. Voller, *Int. J. Heat Mass Transfer*, **40**, 2859 (1997).
28. V. Alexiades and A. D. Solomon, *Mathematical Modeling of Melting and Freezing Processes*, Hemisphere, Washington (1993).
29. K. Aziz and A. Settari, *Petroleum Reservoir Simulation*, Applied Science, London (1979).
30. T. Ertekin, J. H. Abou-Kassem, and G. R. King, *Basic Applied Reservoir Simulation*, Society of Petroleum Engineers, Richardson, TX (2001).
31. M. W. Farthing, C. E. Kees, T. S. Coffey, C. T. Kelley, and C. T. Miller, *Adv. Water Resour.*, **26**, 833 (2003).
32. P. A. Forsyth, Y. S. Wu, and K. Pruess, *Adv. Water Resour.*, **18**, 25 (1995).
33. M. Putti and C. Paniconi, *Adv. Water Resour.*, **18**, 159 (1995).
34. H. Class, R. Helming, and P. Bastian, *Adv. Water Resour.*, **25**, 533 (2002).
35. W. H. Press, S. A. Teukolsky, W. T. Vetterling, and B. P. Flannery, *Numerical Recipes in Fortran 77: The Art of Scientific Computing*, 2nd ed., p. 376, Cambridge University Press, New York (2001).
36. C. T. Kelly, *Solving Nonlinear Equations with Newton's Method*, Society of Industrial and Applied Mathematics, Philadelphia, PA (2003).
37. N. A. De Nora, Inc., *Low Temperature ELAT GDL Microporous Layer on Woven Web* (2005).
38. M. M. Mench, D. J. Burford, and T. W. Davis, in *Proceedings of 2003 ASME International Mechanical Engineering Congress, Heat Transfer Division*, p. 415, The American Society of Mechanical Engineers, New York (2003).
39. M. Khandelwal and M. M. Mench, *J. Power Sources*, **161**, 1106 (2006).
40. J. P. G. Loch, *Soil Sci.*, **126**, 77 (1978).
41. Y. S. Kim, L. Dong, M. A. Hickner, T. E. Glass, V. Webb, and J. E. McGrath, *Macromolecules*, **36**, 6281 (2003).
42. A. Z. Weber and J. Newman, *J. Electrochem. Soc.*, **151**, A311 (2004).

43. M. Pineri, G. Gebel, R. J. Davies, and O. Diat, *J. Power Sources*, In press.
44. R. Bradean, H. Haas, K. Eggen, C. Richards, and T. Vrba, *ECS Trans.*, **3**(1), 1159 (2006).
45. R. Zaffou, J. S. Yi, H. R. Kunz, and J. M. Fenton, *Electrochem. Solid-State Lett.*, **9**, A418 (2006).
46. A. Turhan, K. Heller, J. S. Brenizer, and M. M. Mench, *J. Power Sources*, **160**, 1195 (2006).
47. J. J. Kowal, A. Turhan, K. Heller, J. S. Brenizer, and M. M. Mench, *J. Electrochem. Soc.*, **153**, A1971 (2006).
48. K. O'Neill and R. D. Miller, *Water Resour. Res.*, **21**, 281 (1985).
49. S. Ge, X. Li, B. Li, and I.-M. Hsing, *J. Electrochem. Soc.*, **152**, A1149 (2005).
50. P. J. S. Vie and S. Kjelstrup, *Electrochim. Acta*, **49**, 1069 (2004).
51. E.I. du Pont de Nemours and Company, http://www.dupont.com/fuelcells (2002).
52. U. Pasaogullari and C. Y. Wang, *J. Electrochem. Soc.*, **151**, A399 (2004).
53. A. Z. Weber and J. Newman, *J. Electrochem. Soc.*, **152**, A677 (2005).